Tomography of the Temporal-Spectral State of Subnatural-Linewidth Single Photons from Atomic Ensembles

Ce Yang,[1] Zhenjie Gu,[1] Peng Chen,[1] Zhongzhong Qin,[3,4] J. F. Chen,[1,3,*] and Weiping Zhang[2,3,†]

[1] *Quantum Institute for Light and Atoms, School of Physics and Materials Science, East China Normal University, Shanghai 200241, China*

[2] *School of Physics and Astronomy, and Tsung-Dao Lee Institute, Shanghai Jiao Tong University, Shanghai 200240, China*

[3] *State Key Laboratory of Quantum Optics and Quantum Optics Devices, Institute of Opto-Electronics, Shanxi University, Taiyuan 030006, China*

[4] *Collaborative Innovation Center of Extreme Optics, Shanxi University, Taiyuan, Shanxi 030006, China*

(Received 14 August 2018; revised manuscript received 25 September 2018; published 6 November 2018)

Subnatural-linewidth single photons are generated from atomic ensembles and temporally reshaped as desired so that their temporal modes are eligible for constructing qubits. However, the photon-counting measurement scheme most commonly used in the time-bin basis does not directly give the complex coefficients between time-bins. On the other hand, a mode-sensitive measurement technique, such as homodyne tomography, is hard to implement since a mode-restricting cavity is not allowed in this reshaped photon source. Here, we utilize a cavity-free homodyne detection scheme for reconstructing the temporal-density matrix for the subnatural-linewidth single photons generated from a cold atomic cloud. The characterization of the pure temporal-spectral state of subnatural-linewidth single photons paves the way for exploiting the temporal-spectral degree of freedom to develop photonic-quantum information processing.

DOI: 10.1103/PhysRevApplied.10.054011

I. INTRODUCTION

In thriving photonic-quantum technologies, single photons are one of the most important carriers with quantum states. Qubits or qudits (states with more than two dimensions) can be encoded in various degrees of freedom, e.g., polarizations, spatial, and temporal-spectral modes. Compared to other degrees of freedom, encoding information in temporal-spectral modes is favorable in long-distance communication through fibers [1–4]. Apart from well-known time-bin qubits [5,6], complete and orthogonal temporal-spectral modes are introduced [7] and being quickly developed, both theoretically and experimentally, based on ultrafast photons produced from spontaneous parametric down conversion (SPDC) [8–10]. However, due to the ultra-broad-band feature of these PDC photons, increasing the spectral modes will inevitably reduce the temporal purity of the single-photon state [10], which is essential in quantum information processing. Following this idea, it is possible to encode quantum information directly in the temporal mode of a single photon with an ultra-long coherence time [11,12]. The purity of the temporal reshaped single photon is preserved to be near unity as long as the detectors' time resolution is below 10% of the coherence time [13,14].

The subnatural-linewidth biphotons and single photons are demonstrated to be produced from spontaneous four-wave mixing (SFWM) in atomic ensembles [15–17]. With electromagnetically-induced transparency (EIT) [18], the temporal length of the biphotons can be tailored from nanoseconds to microseconds, and the biphoton generation scheme shows a great advantage in single-photon waveform manipulation [19–24]. The conventional scheme for measuring the temporal mode of these photons is the photon-counting technique, which gives the amplitude of the mode function but not the phase. The phase information of a biphoton is reported through two-photon interference in specific setups [25–28], and recently has been drawn from stimulated emission with seed injection [29]. A general characterization scheme is needed. It is well known that homodyne tomography is widely used to measure the Wigner function of SPDC photons [30–32]. It requires a reference beam to serve as the local oscillator (LO) in the measurement, and is able to provide more information in the temporal-spectral mode. However, this is a mode-sensitive technique so that even the narrow-band single photons from atomic ensembles are restricted by cavity modes [33–35] for mode matching with the LO.

*jfchen@phy.ecnu.edu.cn
†wpz@sjtu.edu.cn

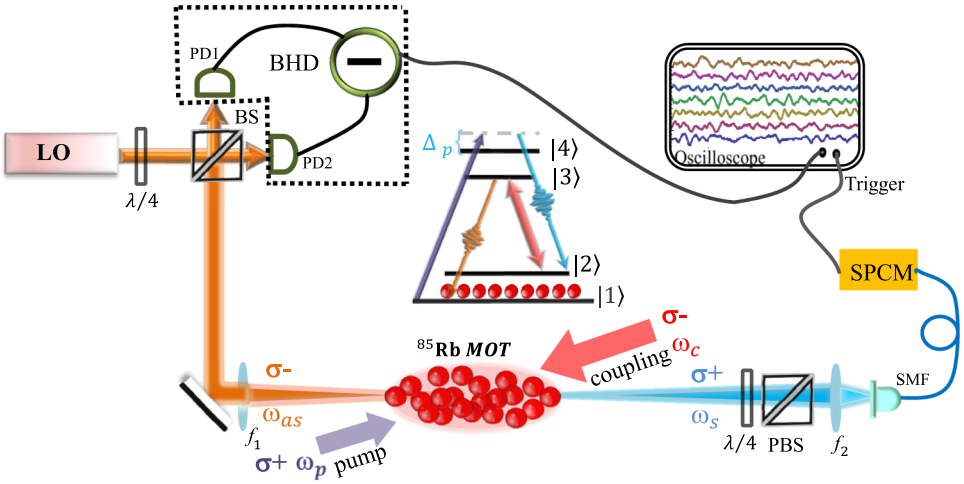

FIG. 1. Schematics of optical setup and atomic-energy level. The paired Stokes and anti-Stokes photons are generated from the SFWM process induced by two classical laser beams (pump and coupling) in a ^{85}Rb cold-atom cloud. The Stokes photons are coupled into single-mode SMF for photon counting. The anti-Stokes photons are directed to a 50/50 beam splitter (BS). A continuous laser with a power of 18 mW, phase locked with the coupling laser, serves as the LO. BHD: balanced homodyne detector. SPCM: single-photon counting module. In the double-Λ energy level scheme, $|1\rangle = 5S_{1/2}, F = 2$, $|2\rangle = 5S_{1/2}, F = 3$, $|3\rangle = 5P_{1/2}, F = 3$ and $|4\rangle = 5P_{3/2}, F = 3$. The coupling laser with Rabi frequency Ω_c is in resonance to the transition $|2\rangle \rightarrow |3\rangle$, and constitutes an EIT energy-level configuration for the anti-Stokes photons.

To achieve various temporal modes for single photons with subnatural linewidths, filters and cavities are abandoned to avoid a predefined spectral mode. In this letter, for the first time, we introduce balanced homodyne detection to measure the complete temporal mode of the subnatural-linewidth single photons without a cavity. The spatial-mode matching between LO and the single-photon source is achievable due to the intrinsic correlation for wavevector k of biphotons. Through homodyne detections with adjustable LO frequencies, we construct the temporal-density matrix of single photons at resolvable time bins. The homodyne-detection approach is uniquely advantageous to measure the temporal-spectral state of subnatural-linewidth single photons, and is shapeable to construct photonic qubits or qudits in a time-frequency degree of freedom.

II. THEORY

We define the temporal mode function (TMF) in the frame of heralded single photons, which is obtained by heralding a partner photon from a photon pair. Assume that we have a pair of frequency-anticorrelated photon pairs, and the two-photon state is denoted as,

$$|1_1, 1_2\rangle_\Phi = \int d\Omega\, \Phi(\Omega)\hat{a}_2^\dagger(\omega_{20} - \Omega)\hat{a}_1^\dagger(\omega_{10} + \Omega)|0\rangle, \tag{1}$$

where $|0\rangle$ denotes the vacuum and ω_{20} and ω_{10} correspond to the central angular frequencies of photons 1 and 2. $\hat{a}_1$ and $\hat{a}_2$ are their corresponding annihilation operators. $\Phi(\Omega)$ is the two-photon joint-spectrum function. After photon 1 is annihilated at time $t = 0$ with its uncertainty infinitesimally small, the heralded single-photon state is expressed as a superposition state,

$$|1\rangle_\Phi = \hat{a}_1(t)|1_1, 1_2\rangle_\Phi, \tag{2}$$

$$= \frac{1}{\sqrt{2\pi}} \int d\Omega\, \Phi(\Omega)\hat{a}_2^\dagger(\omega_{20} - \Omega)|0\rangle. \tag{3}$$

Equivalently, the heralded single-photon state can be expressed as a superposition state of relative arrival times of τ,

$$|1\rangle_\Phi = \int d\tau\, \varphi(\tau)\hat{a}_2^\dagger(\tau)e^{-i\omega_{20}\tau}|0\rangle, \tag{4}$$

where the TMF $\varphi(\tau) = (1/\sqrt{2\pi}) \int d\Omega\, \Phi(\Omega)e^{-i\Omega\tau}$ is the Fourier transform of the joint-spectrum function, and normally this TMF is a complex function with magnitude $|\varphi(\tau)|$ and phase $\theta(\tau) = \arctan[\mathrm{Im}(\varphi(\tau))/\mathrm{Re}(\varphi(\tau))]$.

The above state can be expressed in a discrete time-bin basis. We denote every resolvable ith time bin as $\tau_i = i\delta\tau$, where $\delta\tau$ denotes the detector's temporal resolution. From $[\hat{a}(\tau_i), \hat{a}^\dagger(\tau_j)] = \delta_{ij}$, $|1_i\rangle = |0_{\tau_1}, 0_{\tau_2}, \ldots, 1_{\tau_i}, 0_{\tau_{i+1}}, \ldots\rangle$, and it denotes a single photon found in a specific time bin. In this time-bin basis, the temporal-density operator is defined as $\hat{\rho}_{\mathrm{TM}} = \sum_{ij} \rho_{ij}|1_j\rangle\langle 1_i|$. For subnatural-linewidth single photons, the temporal-density operator can be constructed from a pure state,

$$\hat{\rho}_{\mathrm{TM}} = |1\rangle_{\Phi\Phi}\langle 1| = \sum_i \sum_j \varphi^*(\tau_i)\varphi(\tau_j)|1_{\tau_j}\rangle\langle 1_{\tau_i}|. \tag{5}$$

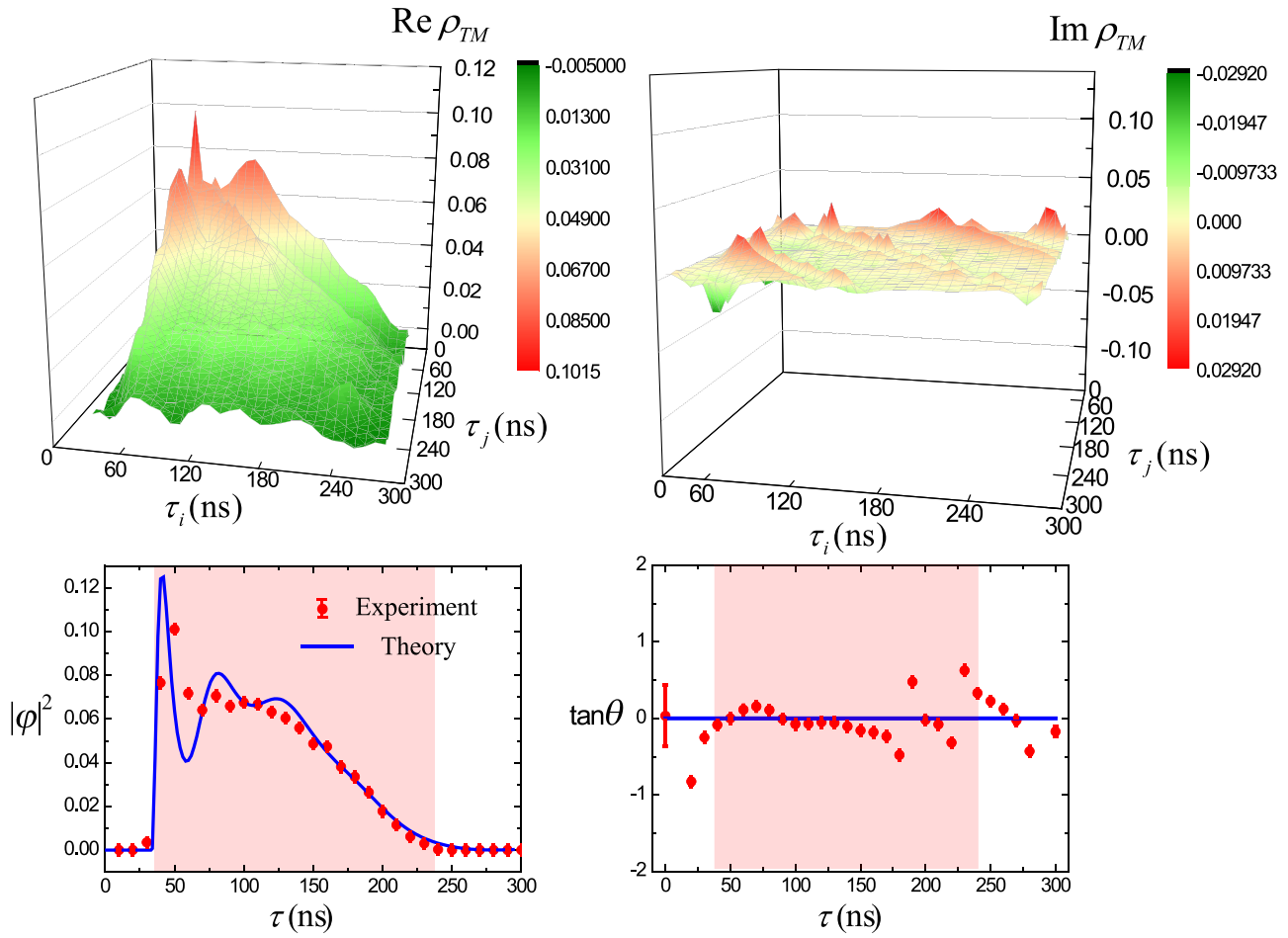

FIG. 2. Temporal-mode characterization of subnatural-linewidth single photons. (a) Real part of the normalized temporal-density matrix, Reρ_{TM}; (b) Imaginary part of the normalized temporal-density matrix, Imρ_{TM}; (c) $|\varphi|^2$, obtained from the diagonal elements at $\tau_i = \tau_j$; (d) $\tan\theta$, obtained from $\mathrm{Im}\rho_{mj}/\mathrm{Re}\rho_{mj}$ where $m = 50$. Here, the value of m is chosen so that ρ_{mj} crosses the maximum value of the matrix. The error bars of (c) are obtained from the standard derivation of the matrix elements σ, i.e., $\sigma = 1/(2\sqrt{N_c})$, in which $N_c = 5 \times 10^5$ is the number of samples taken to obtain the matrix results. The error bars of (d) are from σ multiplied by $\partial(\tan\theta)/\partial\varphi$. In the SFWM process where subnatural-linewidth single photons are generated, $\Omega_c = 2\pi \times 18$ MHz, $\eta = 53$, where η denotes atomic optical depth. The time resolution of BHD used in this measurement is 30 ns.

In the discrete time-bin basis, the matrix elements $\rho_{ij} = \varphi^*(\tau_i)\varphi(\tau_j)$. Therefore, the reconstructed the temporal-density matrix has nontrivial off-diagonal elements, and its diagonal elements constitute the square of the function magnitude $|\varphi(\tau)|^2$.

III. MEASUREMENT SETUPS

The schematics for measuring the temporal mode of single photons is shown in Fig. 1. A pair of spectral anticorrelated photons, Stokes and anti-Stokes, are generated from the SFWM process in a two-dimensional ^{85}Rb magneto-optical trap (MOT) [36,37]. Two cw lasers in the SFWM are a 780 nm pump, which is blue-detuned from $|1\rangle$ to $|4\rangle$ by 146 MHz, and a 795 nm coupling resonant with $|2\rangle \rightarrow |3\rangle$. They are simultaneously applied onto the atom cloud in a backward scattering configuration, and the pump-coupling axis is deviated from the longitudinal axis of the 2D MOT by 2.5°. The pump and coupling beams are circularly polarized, corresponding to σ^+ and σ^-, respectively, and therefore the induced Stokes and anti-Stokes photons are collected with σ^+ and σ^-, respectively. To ensure a low excitation rate of the SFWM, the Rabi frequency of the pump beam is set as $\Omega_p = 2\pi \times 3.3$ MHz and the count rates of the Stokes and anti-Stokes photons are 4400/s and 4000/s, respectively. We utilize a continuous 795 nm laser beam which is phase locked with the coupling laser of the SFWM process to serve as the LO. The polarization and spatial mode of the LO are carefully matched with those of the anti-Stokes traveling in free-space. Even without a cavity for mode restriction, as ascribed to the wavevector correlation for biphotons,

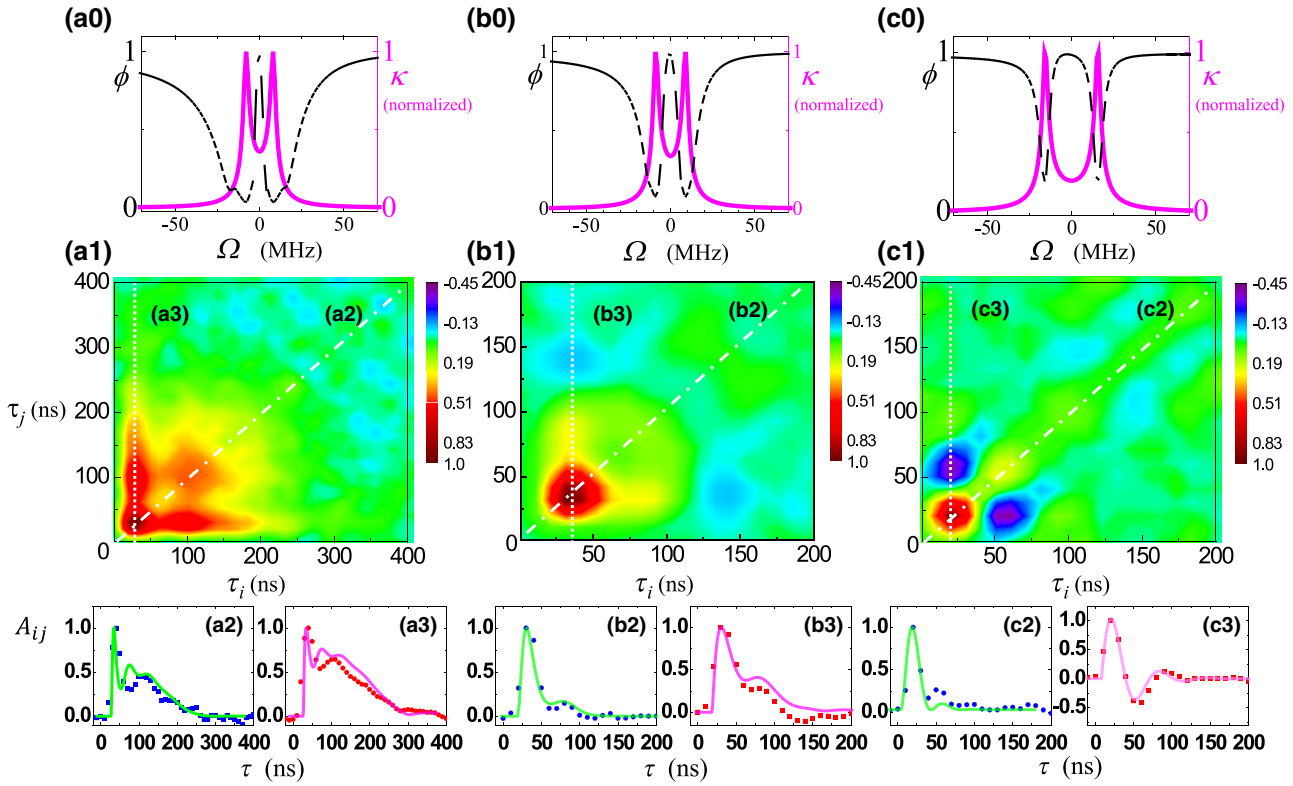

FIG. 3. Reduced autocorrelation A_{ij} measured from homodyne detection. Column (a) $\eta = 53$, $\Omega_c = 2\pi \times 16.5$ MHz; (b) $\eta = 25$, $\Omega_c = 2\pi \times 18$ MHz; (c) $OD = 10$, $\Omega_c = 2\pi \times 31.5$ MHz. The corresponding $\kappa(\Omega)$ and $\Phi(\Omega)$ functions with these three groups of parameters are shown in (a0), (b0), and (c0). The elements along the diagonal axis are plotted in (2), while the elements along a vertical axis which crosses the maximum value are plotted in (3). The solid lines in the plots from (a2) to (c3) are the theoretical curves according to the listed experimental parameters. The maximum element is normalized to be 1. The time resolution $\delta\tau$ is 10 ns.

we mimic the spatial mode of the anti-Stokes beam with a visible laser beam emitted from the single-mode fiber (SMF) collecting the Stokes. The photocurrent of the balance homodyne detection (BHD) is proportional to the quadrature $\hat{X} = (\hat{a}e^{-i\vartheta} + \hat{a}^{\dagger}e^{i\vartheta})/\sqrt{2}$ of the anti-Stokes, where ϑ is the global phase of the single photon. For a heralded single-photon source, the quadrature should be measured with triggers of the Stokes photons, which are detected by a single-photon counting module (SPCM). The time resolution of SPCM is 1 ns, which is far less than the coherence time of the single photons. Therefore, we obtain $\langle\hat{X}(\tau)\rangle$ from about 4000 traces of current samples per second through a high-speed digital oscilloscope trigged by the Stokes photons. To have a significant SNR for TMF measurement, we generally need 10^5 current samples.

IV. RESULTS

The correlation between different time bins can be expressed as $\langle X_i X_j\rangle = \delta_{ij}/2 + A_{ij}$, where $\delta_{ij}/2$ ($\delta_{ij} = 1$ only when $i = j$) denotes the autocorrelation matrix for the vacuum. A_{ij} is the reduced autocorrelation matrix [35] for the anti-Stokes photons with a trigger of a Stokes photon, and is related to the temporal-density matrix as,

$$\begin{aligned} A_{ij} &= \mathrm{Re}[\rho_{\mathrm{TM},ij}]\cos[\Delta\omega(t_i - t_j)] \\ &\quad + \mathrm{Im}[\rho_{\mathrm{TM},ij}]\sin[\Delta\omega(t_i - t_j)] \end{aligned} \tag{6}$$

$\Delta\omega$ is the frequency difference between LO and the anti-Stokes photons. The detailed derivation of Eq. (6) is in the Appendix. With BHD, i.e., $\Delta\omega = 0$, $\mathrm{Re}[\rho_{\mathrm{TM},ij}]$ is directly obtained from A_{ij}. With homodyne detections with adjustable-LO frequencies, i.e., $\Delta\omega \neq 0$, $\mathrm{Im}[\rho_{\mathrm{TM},ij}]$ can be obtained from two pairs of A_{ij} and $\Delta\omega$. To minimize statistical uncertainty, we choose eight sets of LO frequencies, which are equivalent to $\Delta\omega = -10$, -5, 0, 3, 8, 13, 18, 23 MHz, to calculate the real and imaginary parts of the temporal-density matrix. Figure 2(a) shows the normalized $\mathrm{Re}[\rho_{\mathrm{TM}}]$, which is calculated through the autocorrelation matrix A_{ij} when $\Delta\omega = 0$. The diagonal elements $i = j$ are obtained through minimizing a cost function, while obeying the normalization condition $\mathrm{Tr}(\rho_{\mathrm{TM}}) = 1$. Here, the cost function is taken as the difference between the left- and right-hand sides of Eq. (6), squared and summed over all pairs (i,j) in eight sets of A_{ij} and $\Delta\omega$. With the real part calculated, the imaginary part is subsequently obtained by further minimizing the cost function.

Figure 2(b) shows the matrix elements of the imaginary part, which are close to but oscillating around 0. This is the first time we reconstruct a temporal-density matrix for the subnatural-linewidth single-photon state. Without cavity confinement, the density matrix directly reflects the temporal-spectral mode of the SFWM inside the atomic ensemble. Accordingly, we calculate the temporal purity $\mathrm{Tr}(\rho_{\mathrm{TM}}^2) = 92.5\%$, which agrees with the results reported before using Hong-Ou-Mandel interference [14].

For these subnatural-linewidth single photons, whose coherence time is far longer than the time resolution of SPCM, it is safe to assume that the photonic-temporal state is well described by Eq. (4). The square of the magnitude of the TMF $|\varphi|^2$ is directly from the diagonal elements of $\mathrm{Re}[\rho_{\mathrm{TM}}]$, as shown in Fig. 2(c). The phase function $\theta(\tau)$ is evaluated from $\tan\theta_j = \mathrm{Im}[\rho_{mj}]/\mathrm{Re}[\rho_{mj}]$, where $m = 50$ is taken in Fig. 2(d). The magnitude of the mode function agrees well with the photon coincidence measured through the photon-counting technique reported elsewhere before [14,16]. More importantly, the phase function over τ is obtained close to 0 within the coherence window of 200 ns (represented in the shaded pink region in Fig. 2), which is much larger than the coherence time corresponding to the natural linewidth of ^{85}Rb atoms. This is predicted by the model of EIT-assisted SFWM [38], but is not able to be verified with coincidence measurement. In particular, the optical precursor [16,21] signifying abrupt dispersion is revealed clearly in the magnitude and the corresponding phase is found to not be changed. One should be aware that the tested photon source is still maintained as a single photon in the Fock state. The nonclassical property is verified by measuring the conditional autocorrelation function $g_c^{(2)} < 1$. Ideally, the single-photon Fock state yields zero while the two-photon Fock state yields $g_c^{(2)} = 0.5$ [17], which serves as the upper bound to justify the single-photon source. For our source, we obtain $g_c^{(2)} = 0.34 \pm 0.01$ with $\Omega_p = 2\pi \times 3.3$ MHz. This $g_c^{(2)}$ can be further reduced to below 0.2 with decreasing Ω_p [14,21], i.e., lower pump excitation.

Operating without a cavity or other filtering process, the single-photon temporal-spectral modes determined by SFWM in the atomic ensemble exhibit multiple patterns. Generally speaking, the two-photon joint-spectrum function $\Phi(\Omega) \propto \kappa(\Omega)\phi(\Omega)$ [38,39]. Here, $\kappa(\Omega)$ is the nonlinear parametric coupling coefficient of the SFWM process, which is determined by the third-order nonlinear susceptibility, and $\phi(\Omega)$ is the longitudinal-detuning function determined by the phase-matching condition Δk. Two distinguished SFWM regimes are defined as follows. The first one is the EIT-delay regime. When the linewidth of $\phi(\Omega)$ is narrow enough that $\kappa(\Omega)$ can be treated as a constant, $\Phi(\Omega) \propto \phi(\Omega)$. As is shown in Fig. 3 (a0), in this regime, the EIT slow-light effect induced by the resonant or near-resonant coupling laser beam dominates the SFWM spectrum. The EIT transparency window has a significant impact on the TMF and extend it to hundreds of nanoseconds. The other regime is the Rabi oscillation regime, where $\phi(\Omega)$ embraces the two peaks of $\kappa(\Omega)$ and $\Phi(\Omega) \propto \kappa(\Omega)$. Figure 3(c0) shows this regime. The double SFWM channels, which are represented by the two spectral peaks of $\kappa(\Omega)$, beat with each other, and this leads to a π-phase change for the TMF. Normally, this π-phase change is unable to be revealed directly in a conventional photon-counting technique. The BHD we introduce here is able to exhibit the change.

As discussed above, the reduced autocorrelation matrix A_{ij} is equivalent to the real part of the temporal-density matrix when $\Delta\omega = 0$, and when τ_i is kept as a constant m from Eq. (6), the reduced autocorrelation function is

$$A_{jj} = |\varphi(\tau_j)|^2, \tag{7}$$

$$A_{mj} = |\varphi(\tau_m)||\varphi(\tau_j)|\cos[\theta(\tau_j) - \theta(\tau_m)]. \tag{8}$$

The matrix elements in Eqs. (7) and (8) are taken along, respectively, a diagonal and a vertical axis (passing through the maximum) of the reduced autocorrelation matrix. The autocorrelation function drawn from the vertical axis displays the phase switch. Fig. 3 shows single-photon temporal-spectral modes in different SFWM regimes. When EIT plays a significant role in the SFWM process, the TMF does not change its phase throughout the coherence time, as is shown by Fig. 3 (a1). By reducing the optical depth of the cloud while increasing Ω_c, the SFWM process transforms from a group-delay regime to a Rabi oscillation regime. Figure 3 (b1) shows an intermediate case, i.e., overdamped Rabi oscillation. Figure 3 (c1) shows the TMF in the Rabi oscillation regime, in which the TMF takes a negative value in the second oscillation period. Plots (a2) to (c3) agree well with the theoretical calculation of the biphoton wavefunctions [38,39]. In particular, for the Rabi oscillation regime, plot (c3) perfectly matches the TMF of $\varphi(\tau) \sim e^{-\gamma_e\tau}\sin[(\Omega_e/2)\tau]$, and plot (c2) matches $|\varphi(\tau)|^2$. Here, $\gamma_e = (\gamma_{13} + \gamma_{12})/2$ and $\Omega_e = \sqrt{\Omega_c^2 - (\gamma_{13} - \gamma_{12})^2}$, where $\gamma_{\mu\nu}$ denotes the dephasing rate between states μ and ν. Compared to the homodyne detection approach, coincidence measurement from photon counting merely gives the plots (a2), (b2), and (c2).

V. CONCLUSION

In summary, we reconstruct the temporal-density matrix of an EIT-reshaped single photon through its homodyne detections with frequency-tunable and strong LO fields. The amplitude and phase of the mode function are obtained accordingly. Furthermore, we show the distinguished temporal modes characteristic of different SFWM regimes. Compared to the photon-counting measurement technique, the homodyne detection scheme provides the complete

temporal-spectral state. Taking advantage of the narrowband feature, the scheme is free from cavities' spectral modes.

Now, the generation, manipulation, and characterization of the temporal-spectral mode of subnatural-linewidth single photons are experimentally complete. The temporal modes of subnatural-linewidth single photons are useful in constructing the orthogonal mode functions, e.g., Hermite-Gaussian functions, directly in the time domain. Ascribed to the narrow linewidth, the photonic state is always pure and conveniently engineered, even through slow modulators.

ACKNOWLEDGMENTS

This work is supported by the National Key Research and Development Program of China under Grant No. 2016YFA0302001, and the National Natural Science Foundation of China through Grants No. 11674100, No. 11654005, and No. 11234003, the Natural Science Foundation of Shanghai Grant No. 16ZR1448200, and Shanghai Rising-Star Program Grant No. 17QA1401300.

APPENDIX: REDUCED AUTOCORRELATION MATRIX

The temporal-density matrix $\hat{\rho}_{\mathrm{TM}}$ refers to the density matrix of the temporal state of anti-Stokes photons, with the heralding of their partner Stokes photons. Let us denote the two-photon state generated from the SFWM process as $|1_s, 1_{as}\rangle$,

$$\hat{\rho}_{\mathrm{TM}} = \sum_t \hat{a}_s(t)|1_s, 1_{as}\rangle\langle 1_s, 1_{as}|\hat{a}_s^\dagger(t). \tag{A1}$$

The summation is over all the possible annihilation times t of Stokes photons. It is actually the reduced-density matrix [32]. The autocorrelation of anti-Stokes photons with the Stokes photons heralded is described by a reduced autocorrelation matrix [35]. In the following, we present the detailed derivation of the reduced autocorrelation matrix and its relation with $\hat{\rho}_{\mathrm{TM}}$. We also show the detailed data processing to obtain the reduced autocorrelation matrix from original photocurrents taken from the BHD measurement.

Assume that a Stokes photon is recorded at time t, and at a later time, denoted as τ, its paired anti-Stokes photon is detected. At every resolvable ith time bin $\tau_i = i\delta\tau$, where $\delta\tau$ denotes the detector's resolution. The state $|1_i\rangle$ represents a single photon found in this specific time bin. The temporal-density operator $\hat{\rho}_{\mathrm{TM}} = \sum_{mn} \rho_{mn}|1_n\rangle\langle 1_m|$, with ρ_{mn}, denotes the complex matrix elements.

From BHD, we obtain the photon current $\hat{I}$ which is proportional to the quadrature $\hat{X}$. At the j th time bin,

$$\hat{X}_j = \left(\hat{a}_j e^{-i\vartheta_j} + \hat{a}_j^\dagger e^{i\vartheta_j}\right)/\sqrt{2}. \tag{A2}$$

$\vartheta_j = \Delta\omega\tau_j + \vartheta_0$ means the difference of phase between the LO and signal, where $\Delta\omega$ is the frequency difference between them and ϑ_0 shows the difference of the phase between the LO and signal at $t = 0$. Thus we could obtain

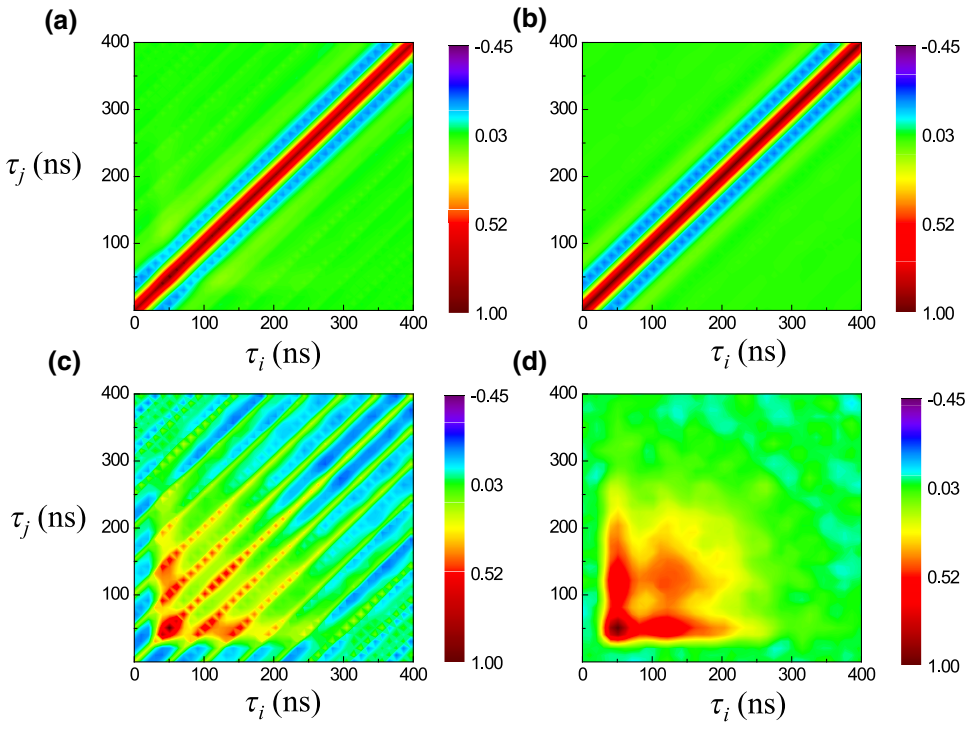

FIG. 4. Autocorrelation matrix of (a) raw photon-current data from BHD; (b) vacuum; (c) raw data subtracted by vacuum; (d) processed data subtracted by thermal noise.

the reduced autocorrelation matrix through the correlation of the photon current:

$$\begin{aligned}\langle \hat{I}_{\tau_i}\hat{I}_{\tau_j}\rangle \propto \langle \hat{X}_i\hat{X}_j\rangle &= \mathrm{Tr}\left[\sum_{mn}\rho_{mn}|1_n\rangle\langle 1_m|\hat{X}_i\hat{X}_j\right]\\ &= \sum_{mnl}\rho_{mn}\langle 1_l|1_m\rangle\langle 1_n|\hat{X}_i\hat{X}_j|1_l\rangle\\ &= \sum_{mn}\rho_{mn}\langle 1_n|\hat{X}_i\hat{X}_j|1_m\rangle. \end{aligned} \tag{A3}$$

To solve the above formula, we need to consider Eq. (A2),

$$\begin{aligned}\langle 1_n|\hat{X}_i\hat{X}_j|1_m\rangle &= \langle 1_n|\hat{X}_i\left[\frac{1}{\sqrt{2}}\left(\hat{a}_j e^{-i\vartheta_j}+\hat{a}_j^\dagger e^{i\vartheta_j}\right)|1_m\rangle\right]\\ &= \frac{1}{\sqrt{2}}\langle 1_n|\frac{1}{\sqrt{2}}\left(\hat{a}_i e^{-i\vartheta_i}+\hat{a}_i^\dagger e^{i\vartheta_i}\right)[e^{-i\Delta\omega t_m}\delta_{jm}|0\rangle\\ &\quad +\sqrt{2}e^{i\Delta\omega t_m}\delta_{jm}|2_m\rangle + e^{i\Delta\omega t_j}\left(1-\delta_{jm}\right)|1_j\,1_m\rangle]\\ &= \frac{1}{2}\langle 1_n|\{e^{-i\Delta\omega(t_m-t_i)}\delta_{jm}|1_i\rangle + 2\delta_{jm}\delta_{im}|1_m\rangle\\ &\quad +(1-\delta_{jm})[\delta_{ij}|1_m\rangle + e^{-i\Delta\omega(t_m-t_j)}\delta_{jm}|1_j\rangle]\}\\ &= \frac{1}{2}\{e^{-i\Delta\omega(t_m-t_i)}\delta_{jm}\delta_{ni}+2\delta_{im}\delta_{jm}\delta_{nm}(1-\delta_{jm})\\ &\quad \times[\delta_{ij}\delta_{nm}+e^{-i\Delta\omega(t_m-t_j)}\delta_{im}\delta_{nj}]\}. \end{aligned} \tag{A4}$$

Therefore, Eq. (A3) becomes

$$\begin{aligned}\langle \hat{X}_i\hat{X}_j\rangle &= \sum_{mn}\rho_{mn}\langle 1_n|\hat{X}_i\hat{X}_j|1_m\rangle\\ &= \frac{1}{2}\sum_{mn}\rho_{mn}\left\{e^{-i\Delta\omega(t_m-t_i)}\delta_{jm}\delta_{ni}+2\delta_{im}\delta_{jm}\delta_{nm}\right.\\ &\quad \left.+\left(1-\delta_{jm}\right)\left[\delta_{ij}\delta_{nm}+e^{-i\Delta\omega(t_m-t_j)}\delta_{im}\delta_{nj}\right]\right\}\\ &= \frac{1}{2}\sum_{mn}[e^{-i\Delta\omega(t_j-t_i)}\delta_{ni}\rho_{jn}+2\delta_{ij}\delta_{nj}\rho_{jn}+\delta_{ij}\rho_{nn}\\ &\quad +e^{-i\Delta\omega(t_i-t_j)}\delta_{nj}\rho_{in}-\delta_{ij}\delta_{nj}\rho_{jn}\\ &\quad -e^{-i\Delta\omega(t_j-t_j)}\delta_{ij}\delta_{nj}\rho_{jn}]\\ &= \frac{1}{2}[e^{-i\Delta\omega(t_j-t_i)}\rho_{ji}+2\delta_{ij}\rho_{jj}+\delta_{ij}\mathrm{Tr}\left[\hat{\rho}\right]\\ &\quad +e^{-i\Delta\omega(t_i-t_j)}\rho_{ij}-\delta_{ij}\rho_{jj}-\delta_{ij}\rho_{jj}]\\ &= \frac{1}{2}\delta_{ij}+\frac{1}{2}[e^{-i\Delta\omega(t_j-t_i)}\rho_{ji}+e^{-i\Delta\omega(t_i-t_j)}\rho_{ij}]\\ &= \frac{1}{2}\delta_{ij}+\mathrm{Re}[\rho_{TM,ij}]\cos[\Delta\omega(t_i-t_j)]\\ &\quad +\mathrm{Im}[\rho_{TM,ij}]\sin[\Delta\omega(t_i-t_j)]\\ &= \frac{1}{2}\delta_{ij}+A_{ij}, \end{aligned} \tag{A5}$$

where $(1/2)\delta_{ij}$ denotes the autocorrelation matrix for the vacuum. After removing the vacuum term, we denote A_{ij} as the reduced autocorrelation matrix for the target optical field.

We acquire the raw result of autocorrelation of the photon current through BHD, as shown in Fig. 4(a), with the case shown in Fig. 3(a) of the main text. With the same setup, Fig. 4(b) shows the autocorrelation matrix of the vacuum. Figure 4(c) corresponds to the result of the removed vacuum, i.e., the result of Figure 4(a) subtracted by (b). However, Figure 4(c) still contains the current background of the detector and the thermal noise of SFWM. They cause Figure 4(c) to be distorted. Fortunately, the current background of the detector and the thermal noise only depend on the difference of two time bins. These noises have the same value along the axis of $t_i - t_j = \text{const}$. In data processing, we record the experimental data in a range far away from the concerned time window, calculate the average value along the axis of $t_i - t_j = \text{const}$, and subtract them from Figure 4(c). Finally, we obtain the reduced autocorrelation matrix A_{ij} as shown in Fig. 4(d).

[1] I. Marcikic, H. deRiedmatten, W. Tittel, H. Zbinden, and N. Gisin, Long-distance teleportation of qubits at telecommunication wavelengths, Nature **421**, 509 (2003).

[2] P. R. Tapster, J. G. Rarity, and P. C. M. Owens, Violation of Bell's Inequality over 4 km of Optical Fiber, Phys. Rev. Lett. **73**, 1923 (1994).

[3] R. T. Thew, S. Tanzilli, W. Tittel, H. Zbinden, and N. Gisin, Experimental investigation of the robustness of partially entangled qubits over 11 km, Phys. Rev. A **66**, 062304 (2002).

[4] H. de Riedmatten, I. Marcikic, W. Tittel, H. Zbinden, D. Collins, and N. Gisin, Long Distance Quantum Teleportation in a Quantum Relay Configuration, Phys. Rev. Lett. **92**, 047904 (2004).

[5] J. D. Franson, Bell Inequality for Position and Time, Phys. Rev. Lett. **62**, 2205 (1989).

[6] P. G. Kwiat, A. M. Steinberg, and R. Y. Chiao, High-visibility interference in a Bell-inequality experiment for energy and time, Phys. Rev. A **47**, R2472 (1993).

[7] B. Brecht, D. V. Reddy, C. Silberhorn, and M. G. Raymer, Photon Temporal Modes: A Complete Framework for Quantum Information Science, Phys. Rev. X **5**, 041017 (2015).

[8] C. K. Law, I. A. Walmsley, and J. H. Eberly, Continuous Frequency Entanglement: Effective Finite Hilbert Space and Entropy Control, Phys. Rev. Lett. **84**, 5304 (2000).

[9] B. Brecht, A. Eckstein, R. Ricken, V. Quiring, H. Suche, L. Sansoni, and C. Silberhorn, Demonstration of coherent time-frequency Schmidt mode selection using dispersion-engineered frequency conversion, Phys. Rev. A **90**, 030302(R) (2014).

[10] V. Ansari, J. M. Donohue, M. Allgaier, L. Sansoni, B. Brecht, J. Roslund, N. Treps, G. Harder, and C. Silberhorn, Tomography and Purification of the Temporal-Mode

Structure of Quantum Light, Phys Rev. Lett. **120**, 213601 (2018).
[11] Z. Han, P. Qian, L. Zhou, J. F. Chen, and W. Zhang, Coherence time limit of the biphotons generated in a dense cold atom cloud, Sci. Rep. **5**, 9126 (2015).
[12] L. Zhao, Y. Su, and S. Du, Narrowband biphoton generation in the group delay regime, Phys. Rev. A **93**, 033815 (2016).
[13] S. Du, Quantum-state purity of heralded single photons produced from frequency-anticorrelated biphotons, Phys. Rev. A **92**, 043836 (2015).
[14] P. Qian, Z. Gu, R. Cao, R. Wen, Z. Y. Ou, J. F. Chen, and W. Zhang, Temporal Purity and Quantum Interference of Single Photons from Two Independent Cold Atomic Ensembles, Phys. Rev. Lett. **117**, 013602 (2016).
[15] V. Balić, D. A. Braje, P. Kolchin, G. Y. Yin, and S. E. Harris, Generation of Paired Photons with Controllable Waveforms, Phys. Rev. Lett. **94**, 183601 (2005).
[16] S. Du, P. Kolchin, C. Belthangady, G. Y. Yin, and S. E. Harris, Subnatural Linewidth Biphotons with Controllable Temporal Length, Phys. Rev. Lett. **100**, 183603 (2008).
[17] C. Shu, P. Chen, T. K. A. Chow, L. Zhu, Y. Xiao, M. M. T. Loy, and S. Du, Subnatural-linewidth biphotons from a Doppler-broadened hot atomic vapour cell, Nat. Commun. **7**, 12783 (2016).
[18] S. E. Harris, Electromagnetically induced transparency, Phys. Today **50**, 36 (1997).
[19] C. Belthangady, S. Du, C.-S. Chuu, G. Y. Yin, and S. E. Harris, Modulation and measurement of time-energy entangled photons, Phys. Rev. A **80**, 031803(R) (2009).
[20] P. Kolchin, C. Belthangady, S. Du, G. Y. Yin, and S. E. Harris, Electro-Optic Modulation of Single Photons, Phys. Rev. Lett. **101**, 103601 (2008).
[21] S. Zhang, J. F. Chen, C. Liu, M. M. T. Loy, G. K. L. Wong, and S. Du, Optical Precursor of a Single Photon, Phys. Rev. Lett. **106**, 243602 (2011).
[22] J. F. Chen, S. Zhang, H. Yan, M. M. T. Loy, G. K. L. Wong, and S. Du, Shaping Biphoton Temporal Waveforms with Modulated Classical Fields, Phys. Rev. Lett. **104**, 183604 (2010).
[23] L. Zhao, X. Guo, Y. Sun, Y. Su, M. M. T. Loy, and S. Du, Shaping the Biphoton Temporal Waveform with Spatial Light Modulation, Phys. Rev. Lett. **115**, 193601 (2015).
[24] Y.-W. Cho, K.-K. Park, J.-C. Lee, and Y.-H. Kim, Engineering Frequency-Time Quantum Correlation of Narrow-Band Biphotons from Cold Atoms, Phys. Rev. Lett. **113**, 063602 (2014).
[25] Federica A. Beduini, Joanna A. Zieliska, Vito G. Lucivero, Yannick A. de Icaza Astiz, and Morgan W. Mitchell, Interferometric Measurement of the Biphoton Wave Function, Phys. Rev. Lett. **113**, 183602 (2014).
[26] N. Tischler, A. Büse, L. G. Helt, M. L. Juan, N. Piro, J. Ghosh, M. J. Steel, and G. Molina-Terriza, Measurement and Shaping of Biphoton Spectral Wave Functions, Phys. Rev. Lett. **115**, 193602 (2015).
[27] P. Chen, C. Shu, X. Guo, M. M. T. Loy, and S. Du, Measuring the Biphoton Temporal Wave Function with Polarization-Dependent and Time-Resolved Two-Photon Interference, Phys. Rev. Lett. **114**, 010401 (2015).
[28] Alex O. C. Davis, Valrian Thiel, Michal Karpiski, and Brian J. Smith, Measuring the Single-Photon Temporal-Spectral Wave Function, Phys. Rev. Lett. **121**, 083602 (2018).
[29] Kwang-Kyoon Park, Jin-Hun Kim, Tian-Ming Zhao, Young-Wook Cho, and Yoon-Ho Kim, Measuring the frequency-time two-photon wavefunction of narrowband entangled photons from cold atoms via stimulated emission, Optica **4**, 1293 (2017).
[30] D. T. Smithey, M. Beck, M. G. Raymer, and A. Faridani, Measurement of the Wigner Distribution and the Density Matrix of a Light Mode using Optical Homodyne Tomography: Application to Squeezed States and the Vacuum, Phys. Rev. Lett. **70**, 1244 (1993).
[31] U. Leonhardt, *Measuring the Quantum State of Light* (Cambridge University Press, Cambridge, 1997).
[32] A. I. Lvovsky and M. G. Raymer, Continuous-variable optical quantum-state tomography, Rev. Mod. Phys. **81**, 299 (2009).
[33] A. MacRae, T. Brannan, R. Achal, and A. I. Lvovsky, Tomography of a High-Purity Narrowband Photon from a Transient Atomic Collective Excitation, Phys. Rev. Lett. **109**, 033601 (2012).
[34] E. Bimbard, R. Boddeda, N. Vitrant, A. Grankin, V. Parigi, J. Stanojevic, A. Ourjoumtsev, and P. Grangier, Homodyne Tomography of a Single Photon Retrieved on Demand from a Cavity-Enhanced Cold Atom Memory, Phys. Rev. Lett. **112**, 033601 (2014).
[35] Z. Qin, A. S. Prasad, T. Brannan, A. MacRae, A Lezama, and A. I. Lvovsky, Complete temporal characterization of a single photon, Light: Science & Applications **4**, e298 (2015).
[36] S. Zhang, J. F. Chen, C. Liu, S. Zhou, M. M. T. Loy, G. K. L. Wong, and S. Du, A dark-line two-dimensional magneto-optical trap of 85Rb atoms with high optical depth, Rev. Sci. Instrum. **83**, 073102 (2012).
[37] J. Zhang, Z.-J. Gu, P. Qian, Z.-G. Han, and J.-F. Chen, Cold atom cloud with high optical depth measured with large duty cycle, Chin. Phys. Lett. **32**, 064211 (2015).
[38] S. Du, J. Wen, and M. H. Rubin, Narrowband biphoton generation near atomic resonance, J. Opt. Soc. Am. B **25**, C98 (2008).
[39] J. F. Chen and S. Du, Narrowband photon pair generation and waveform reshaping, Front. Phys. **7**, 494 (2012).